

Performance evaluation of
Flight-Model Si-Pad sensors for
Soft Gamma-ray Detector (SGD)
onboard ASTRO-H

PARK INCHUN

M103287

High Energy · Optic & Infrared Astrophysics Laboratory

Graduate School of Science

HIROSHIMA UNIVERSITY

2012. 2. 10

Contents

1	Introduction	1
1.1	High Energy Astronomy	1
1.2	ASTRO-H	2
1.2.1	Development background and Mission purpose	2
1.2.2	Specification of Mission Instruments	3
1.2.3	Other missions of high-energy astronomy	6
1.3	Purpose of This Thesis	9
2	Soft Gamma-ray Detector:SGD	11
2.1	System of SGD	11
2.1.1	Compton Camera	12
2.2	Science of SGD	12
2.3	Pixel-shaped Si detector:Si-Pad	13
2.3.1	Characteristics of the Si-Pad	15
2.3.2	Status of SGD Si-Pad	17
2.4	Process of multi-channel signal acquirement	17
2.4.1	Principal of signal acquirement	17
2.4.2	Front end signal process	18
3	Ranking of Flight Model Si-Pad sensors for SGD	19
3.1	HPK data	19
3.2	Ranking	20
4	Performance Evaluation of Si-Pad sensors with ASIC	25
4.1	Items of Performance Evaluation	25
4.1.1	Dependence on Bias High Voltage	25
4.1.2	Temperature Dependence	25
4.2	Expected Result of the PFM Si-Pad sensors	26
4.2.1	Multi-channel readout of PFM Si-Pad with VA450.3	26
4.2.2	Single-channel readout with FM Si-Pad sensor	30
4.3	Results on the FM Si-Pad sensor	32
4.3.1	Experiment Setup	32
4.3.2	High voltage dependency	32
4.3.3	Temperature Dependency	35
5	Consideration	39
	Bibliography	41

Introduction

Contents

1.1 High Energy Astronomy	1
1.2 ASTRO-H	2
1.2.1 Development background and Mission purpose	2
1.2.2 Specification of Mission Instruments	3
1.2.3 Other missions of high-energy astronomy	6
1.3 Purpose of This Thesis	9

1.1 High Energy Astronomy

The progression of science has always been hand in hand with technological development. Development of the telescope changed the paradigm of space. In astronomy, starting in the later half of the 20th century, technology development has enabled wider frequency observations (such as radio, infrared, X-ray) above optical ones. Especially, rocket and satellite technologies have enabled us to observe with X-ray and Gamma-ray which is absorbed by atmosphere, and led the way to the birth of the new science field of High Energy Astronomy. In 1962, when the rocket Aerobee discovered that the star Scorpius X-1 was actually shining under X-ray exposure, X-ray astronomy have started. X-ray observations via satellites have begun in the United States in 1970s.



Figure 1.1: From the left picture, Chandra[1], XMM-Newton[2], Suzaku[3]

Right now, there are many active X-ray satellites including NASA's Chandra, ESA's XMM-Newton and INTEGRAL. Japan has started on this field with Hakucho (CORSA-b) in 1979, and has launched five satellites since then, and the latest satellite is Suzaku (ASTRO-E2). ASTRO-H is developing as a next generation

of X-ray observatory satellite. In this thesis, We treat of Si sensors that are used for the Soft Gamma-ray Detector(SGD), one of ASTRO-H's science instruments.

1.2 ASTRO-H

1.2.1 Development background and Mission purpose

Since the beginning of High-energy astronomy, numerous X-ray observation satellites were launched. Thanks to high-quality X-ray images taken by Chandra and XMM-Newton at the in 2000s, there has been a significant progress in High-energy astrophysics. However, these satellites are both over ten years old. Considering the development of new observation equipment and the general aging of the satellite itself, the operational lifetimes of these satellites are almost over, and a new X-ray observatory satellite is needed. Japan has been working on new observation techniques, and has launched many satellites for X-ray observation. Using its accumulated experience in the X-ray astrophysics field, Japan has started working on a plan for NeXT (Next X-ray Telescope) as the follower of Suzaku, which was launched in 2005. This plan (NeXT) contains four significant instruments planted in it: First one is a micro calorimeter named Soft X-ray Spectrometer. Second one is a Hard X-ray Imager. Third one is Soft X-ray Imager. It has X-ray CCD system to make image. And the fourth one is a Soft Gamma-ray Detector.



Figure 1.2: Concept image of ASTRO-H[4]

The NeXT plan was later renamed as ASTRO-H, and it is planned to be launched in 2014. To fulfill this project, ISAS-JAXA (leader of the ASTRO-H project), many Japanese universities, and many international research institutions such as NASA are working together. Even though the main purpose of ASTRO-H is to investigate the structure and the evolution of the universe, ASTRO-H will also observe black

holes, supernova explosions and cluster of galaxies filled with high temperature plasma and undoubtedly provide valuable information. The instruments to be used in this project are introduced in more detail in the next section.

1.2.2 Specification of Mission Instruments

ASTRO-H will load 4 sets of mission instruments.

- SXS(Soft X-ray Spectrometer)

The Soft X-ray Spectrometer (SXS) consists of the Soft X-ray Telescope (SXT-S), the X-ray Calorimeter Spectrometer (XCS) and the cooling system. The XCS is a 32-channel system with an energy resolution of 7 eV in 0.3-12 keV. Micromachined, ion-implanted silicon is the basis of the thermistor array, and 8-micron-thick HgTe absorbers provide high quantum efficiency across the 0.3-12-keV band. With a 6-m focal length, the 0.83 mm pixel pitch corresponds to 0.48 arcmin, giving the array a field of view of 2.85 arcmin on a side. In order to obtain high energy resolution, the XCS cooling system must cool the array to 50 mK.

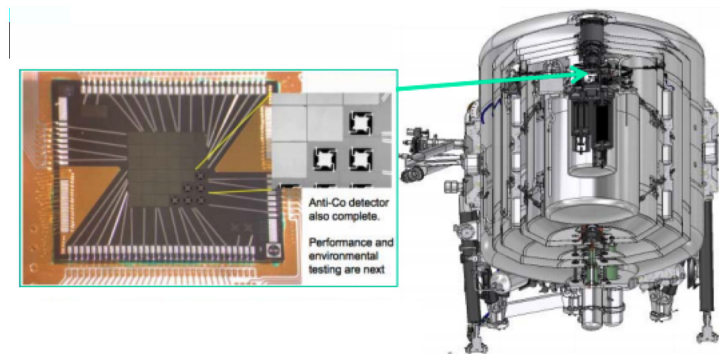


Figure 1.3: XCS[5]

The SXS science objectives require a mirror with larger effective area than those flown on Suzaku, especially in the Fe K band. The SXS effective area at 6 keV is 210 cm², a 60 percent increase over the Suzaku XRS, while at 1-keV the SXS has 160 cm², a 20 percent increase. If we adopt a thin filter, the effective area at 1 keV increases to +250-cm². The required angular resolution is 1.7 arcmin, HPD, comparable to the orbit performance of the mirrors on Suzaku.

SXS uniquely performs high-resolution spectroscopy of extended sources. In contrast to a grating, the spectral resolution of the calorimeter is unaffected by source size because it is non-dispersive. SXS makes possible high-resolution spectroscopy of sources inaccessible to current grating instruments.

- SXI(Soft X-ray Imager)

X-ray sensitive silicon charge-coupled devices (CCDs) are a nominal device for the X-ray astronomy. The low background and high energy resolution achieved with the XIS/Suzaku clearly show that the X-ray CCD will also play very important role in the ASTRO-H mission. Soft X-ray imaging system consists of an imaging mirror (SXT-I) and a CCD camera.



Figure 1.4: CCD of SXI[5]

The SXI will use next generation Hamamatsu CCD chips with a thick depletion layer, low noise, and almost no cosmetic defects. The SXI features a large FOV and covers 35×35 arcmin² region on the sky, complementing the smaller FOV but much higher spectral resolution of the SXS calorimeter. A mechanical cooler ensures a long operational life at -120 degree. The overall quantum efficiency and spectral resolution is better than the Suzaku XIS. The imaging mirror has a 6-m focal length, and a diameter no larger than 45 cm.

- HXI(Hard X-ray Imager)

The hard X-ray imaging system onboard ASTRO-H consists of two identical mirror-detector pairs (Hard X-ray Telescope (HXT) and Hard X-ray Imager (HXI)). The HXT has conical-foil mirrors with graded multilayer reflecting surfaces that provide a 5-80 keV energy range. The effective area of the HXT is maximized for a long focal length, with current design value of 12 m giving an effective area of 300 cm² at 30 keV. A depth-graded multi-layer mirror reflects X-rays not only by total external reflection but also by Bragg reflection. In order to obtain high reflectivity up to 80 keV, the HXT consists of a stack of multi-layers with different sets of periodic length and number of layer pairs with a carbon/platinum coating.

The HXI consists of four-layers of 0.5-mm-thick Double-sided Silicon Strip Detectors (DSSD) and one layer of 0.5 1-mm-thick CdTe imaging detector. In this configuration, soft X-ray photons will be absorbed in the Si part (DSSD), while hard X-ray photons go through the Si part and are detected by the newly developed CdTe double strip detector. Silicon strip detector and CdTe strip detector are us to placed inside very deep well of the active shield made of

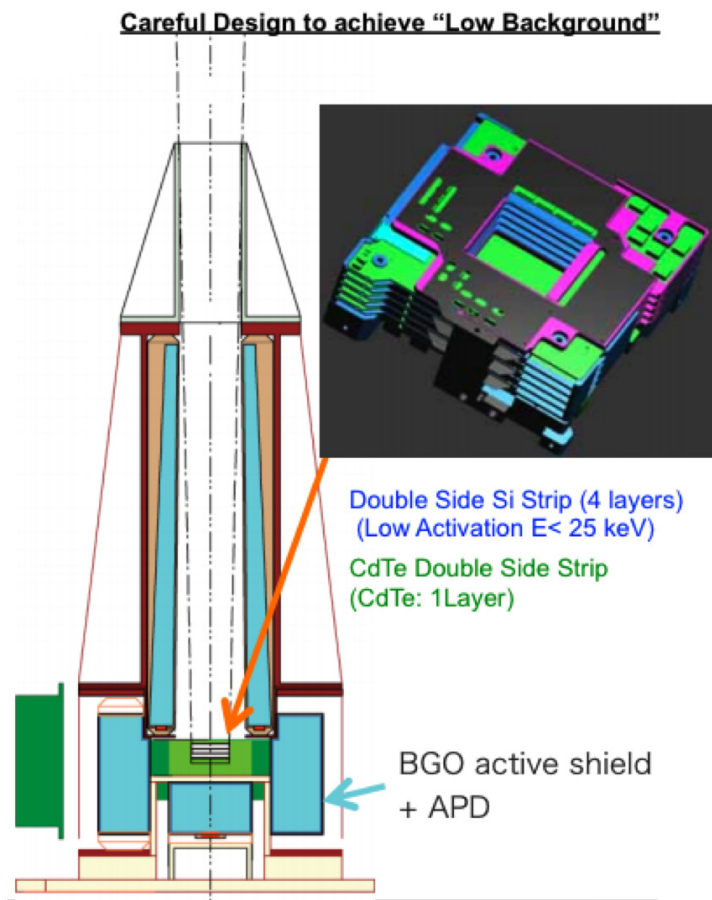


Figure 1.5: Specification of HXI focal plane detector[7]

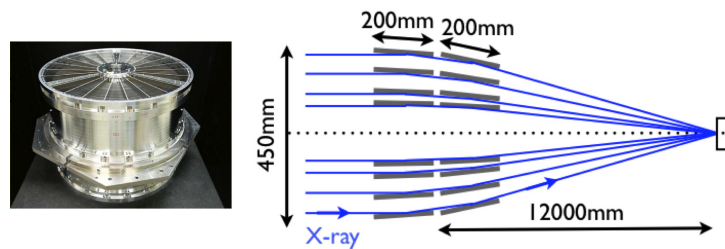


Figure 1.6: HXT[8]

BGO ($\text{Bi}_4\text{G}_3\text{O}_{12}$). Signal from the BGO shield is used to reject background events. The total thickness of the four DSSDs is 2 mm, the same as that of the PIN detector of the HXD onboard Suzaku. The DSSDs cover the energy below 30 keV while the CdTe strip detector covers the 20-80 keV band.

- SGD(Soft Gamma-ray Detector)

The SGD is a non-focusing soft gamma-ray detector with a 10-600 keV energy range and sensitivity at 300keV, more than 10 times better than the Suzaku HXD (Hard X-ray Detector). It outperforms previous soft-Gamma-ray instruments in background rejection capability by adopting a new concept of narrow-FOV Compton telescope.

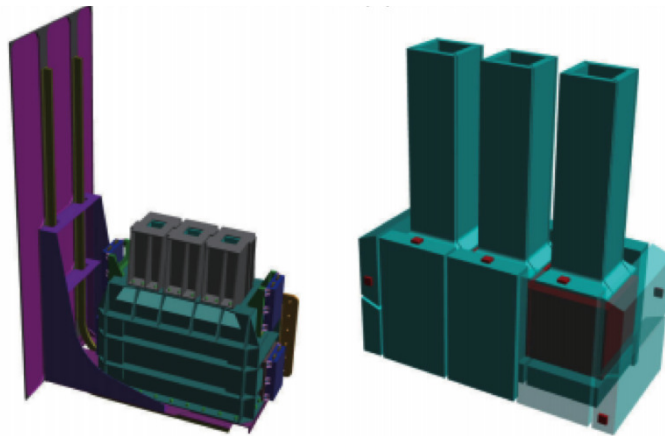


Figure 1.7: Concept of SGD[9]

In order to lower the background dramatically and thus to improve the sensitivity as compared to the HXD of Suzaku, we combine a stack of Si-Pad and CdTe pixel detectors to form a Compton telescope. The telescope is then mounted inside the bottom of a well-type BGO active shield. Above 50 keV, we can require each event to interact twice in the stacked detector, once by Compton scattering in a stack of Si-Pad sensors, and then by photo-absorption in the CdTe part (Compton mode). Once the locations and energies of the two interactions are measured, the Compton kinematics allows us to calculate the energy and direction (as a cone in the sky) of the incident gamma-ray by following the Compton equation. We only select events that are consistent with gamma-rays coming from the FOV of collimator (Narrow FOV Compton telescope).

1.2.3 Other missions of high-energy astronomy

In high-energy astronomy field, there are other satellite missions planned to be launched. Characteristics of those missions are commented in the following.

- NuSTAR(Nuclear Spectroscopic Telescope Array)
NuSTAR is an image detector developed by California Institute of Technology (Caltech). Like HXI, it observes hard X-ray (5-79keV). NuSTAR will be placed in the Pegasus rocket and Air launched in March, 2012. If NuSTAR succeeds in its mission, it will be the first image detector operating in hard X-ray band. NuSTAR has the focal length of 10 meters to help focus on hard X-ray. The CdZnTe detector of NuSTAR is thick in 600um with 32x32 pixels. Also to reduce background signal, the CdZnTe detector is covered with CsI detector.

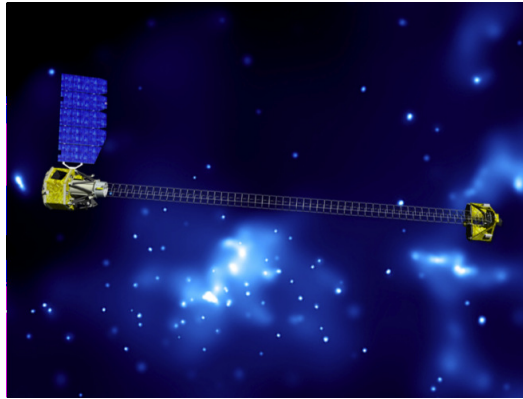


Figure 1.8: NuSTAR[11]

- GEMS(Gravity and Extreme Magnetism SMEX)
GEMS project has been developed under the leadership of NASA. GEMS satellite can observe X-ray polarization under 10keV. This means almost a hundred times higher sensitivity than the conventional polarization observation devices. It uses gas detectors to track the photons and measure polarization. GEMS is expected to be launched in July, 2014.
- NHXM(New Hard X-ray Imaging and Polarimetric Satellite Mission)
Led by ESA, many European countries collaborat for developing a 0.2-80keV X-Ray observation satellite. NHXM has some similar characteristics with the ASTRO-H satellite, such as the energy band and the detectors. However, the effective area of NHXM is twice bigger than that of ASTRO-H. NHXM uses CCD detector for soft X-ray detection and CdTe detector for hard X-ray detection. NHXM also has a Gas Pixel Detector (GPD), which is already fully developed, that measures soft X-ray polarization. It is expected to be launched in 2016.
- HXMT(Hard X-ray Modulation Telescope)
China is building this telescope with the purpose of all-sky X-ray observation. With three energy detectors, this telescope covers the energy range of 1-250keV. It is planned to be launched in 2012.



Figure 1.9: GEMS[12]

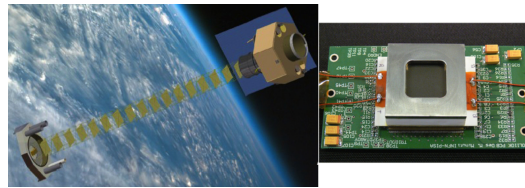


Figure 1.10: NHXM and GPD[13]

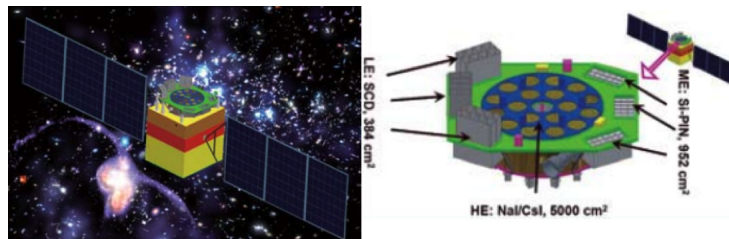


Figure 1.11: HXMT and detectors[14]

- GRI(Gamma-Ray Imager)

ESA is planning to develop an imager to capture the space-born gamma-rays. However, since gamma-rays are hard to focus ,requiring no less than a hundred meters to focus, GRI will be making formation flight. The project is expected to take place between 2015 and 2025.

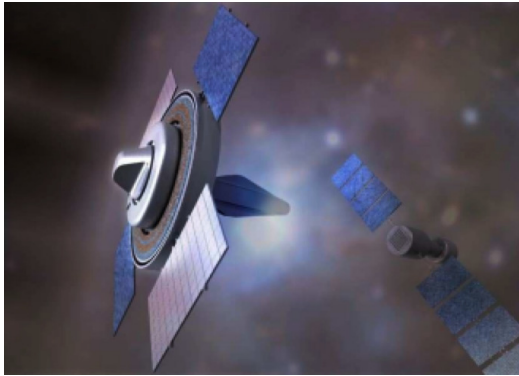


Figure 1.12: GRI[15]

- MEGA(Medium Energy Gamma-ray Astronomy telescope)

This gamma-ray detector is being developed by Max Planck Institute. It is similar to the Compton camera of SGD. MEGA uses Double-side Si Detector (DSSD) as tracker and CsI as calorimeter. Even though the ground testing is done and its performance was confirmed, there are still no concrete announcements regarding its launch.

1.3 Purpose of This Thesis

This thesis investigates the characteristics of Si-Pad sensor, which is the main sensor operating in SGD. The Si-Pad sensor used in this research is a fully developed, finalized version Flight Model (FM). The study focuses on the performance evaluation and classification of these sensors before they are mounted on the actual satellite. Leak current is used to distinguish the high quality sensors within the already been manufactured FM Si-Pad sensors. Finally, this research tries to find out whether the Si-Pad sensors would work despite the negative effects of gamma-rays and proton radiation in the orbit.

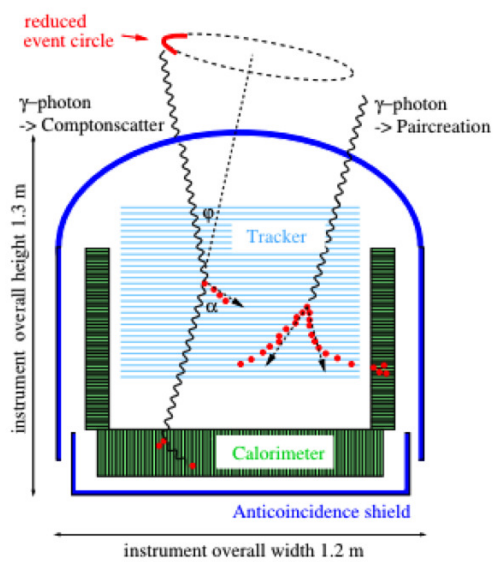


Figure 1.13: Principle of MEGA Compton camera[16]

Soft Gamma-ray Detector:SGD

Contents

2.1	System of SGD	11
2.1.1	Compton Camera	12
2.2	Science of SGD	12
2.3	Pixel-shaped Si detector:Si-Pad	13
2.3.1	Characteristics of the Si-Pad	15
2.3.2	Status of SGD Si-Pad	17
2.4	Process of multi-channel signal acquirement	17
2.4.1	Principal of signal acquirement	17
2.4.2	Front end signal process	18

2.1 System of SGD

ASTRO-H has a high energy photon detector which is called a Soft Gamma-ray Detector (SGD). SGD represents the next generation of X-ray observation following the HXD in Suzaku. SGD, unlike other focusing detectors, is not coupled with a telescope mirror. It detects photons directly from the astronomical object. Yet, in this energy band, it is a significant problem to detect photons because of the background signals. To reduce the background signals, SGD uses active shield and Compton camera. By using these methods, it becomes possible to detect photons effectively. These two methods will be explained in detail in the following subchapter.

SGD has two units which are installed at side panels. Each unit has three Compton cameras surrounded by active shields. Since SGD is attached to the outside of a satellite, it is designed to stand for severe environment conditions in space such as cosmic rays and temperature changes. The detectable energy of a photon is between 10-600keV which is called a soft gamma-ray. this observation range is widen the ASTRO-H's multi-wave observation ability, and help to get more information about target objects. Observation by Compton camera has not only ability of spectrometer, but also ability of polarimetric device. Polarized photons come into Compton camera and are scattered by Si into restricted direction. Knowing this direction, we can measure polarization of photon. If this measurement succeeds, it might be the first polarization observation of soft gamma-rays.

SGD is designed as a space telescope, observing space objects. Still, its technology can be used to develop devices for other radiation related fields like medical, to detect radiation contamination.

2.1.1 Compton Camera

The photon tracking device, called compton camera, catch movement of photon that is interact with matter by compton scattering. To track and find where photon comes from, the compton camera need to measure two place of photon's position and energy. The one is photon scattered and the other is absorbed. In SGD, two kind of sensor, Si and CdTe, combined to perform as compton. when photon come into compton camera, Si sensor scattering photon and after that scattered photon absorbed CdTe sensor. The reason of use these sensors is that each component have characteristic of compton scattering and photoelectric absorption for soft gamma-ray. One compton camera stack 32 piece of Si sensors, and under the Si sensor, 8 piece CdTe sensor stacked. and 1stack of CdTe sensor cover side of compton camera. One sensor have 256 pad-shaped channels, to find where photon respond. Each channel output electronic signal when photon react with matter. this analog signals have processed by ASIC. ASIC composed ability of pre-amp, shape-amp and ADC. One ASIC can process signal from 64 channels.

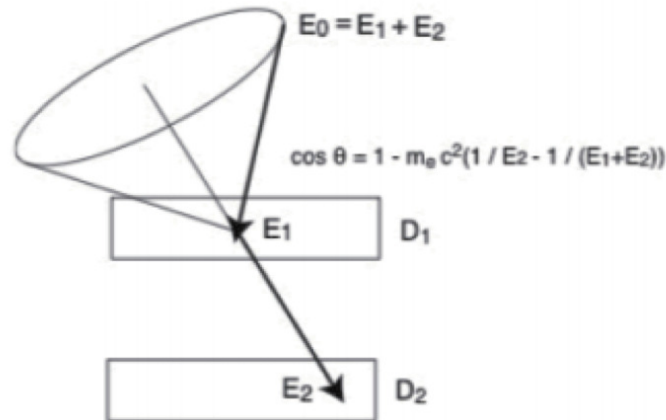


Figure 2.1: Principle of Compton camera

2.2 Science of SGD

In the space observations done with X-rays and Gamma-rays, new discoveries were made in matters which cannot be explained with thermal dynamics. The need to understand these phenomena has led to the birth of High Energy Astrophysics. Close to Earth, there are solar flares, pulsars, X-ray binary stars and supernova remnants.

At distant galaxies, there are active galactic nuclei and gamma-ray bursts. These are also called cosmic accelerators whose high-energy particles contain higher energy than the energy that is created in the particle accelerators in the world. High energy astrophysics can help us to understand not just the process of cosmic evolution or the structure of the universe, but it also helps us to understand a variety of science fields like the research on the origin of matter. However, due to the technological constraints of the observation equipment and the low occurrence rate of astronomical phenomena, non-thermal astronomical phenomena are still not known in full details.

The followings are some example descriptions of astronomical phenomena that can be explained via Soft Gamma-ray Detector (SGD) observation.

- High-energy cosmic ray

Since the observation of high-energy particles has started in the mid-twentieth century, high-energy particles that are over several MeV have been mainly discovered in space. In these cosmic rays, some high-energy cosmic rays that have energy levels above the theoretical predictions have been discovered. The source of these rays has been a mystery for many years. In recent studies, Active Galactic Nuclei (AGN) that are found in the center of giant black holes in distant galaxies were claimed to be the source of these very high-energy cosmic rays. In addition to AGN, radiation from shockwave of interstellar medium and gamma-ray bursts are listed as possible sources. High-energy cosmic ray research is also closely associated with the study of dark matter. Clarifying the nature of the dark matter has become an important issue for high-energy astrophysics.

- Relativistic jet

Through radio or X-ray observation, relativistic plasma outflow of plasma particles from radio galaxies or quasars can be observed. This is called jet. Supermassive black holes are believed to be the sources of these jets which are collimated by the spiral-shaped magnetic field. Inverse Compton scattering of photons from the jet, and the emission of synchrotron radiation can be observed through radio to gamma-rays.

Since information about the magnetic field in jets is measured via polarization observation, the superior polarization capability of the SGD is important for understanding the relativistic jet.

2.3 Pixel-shaped Si detector:Si-Pad

In this section, we describe Si-Pad sensors used for the SGD. Si sensors are widely used in particle accelerators and X-ray spectrometers. Numerous studies were done to find ways for this sensor to show stable performance as a detector. Our high-energy astrophysics laboratory is developing a Si-Pad sensor based on the experience gained from developing the Si-Strip Detector (SSD) for the Large Area Telescope (LAT) which is onboard Fermi gamma-ray telescope that was launched in 2008.

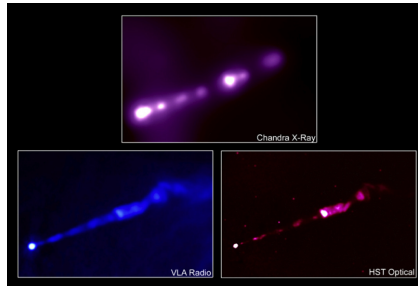


Figure 2.2: Example of jet



Figure 2.3: GLAST and SSD

2.3.1 Characteristics of the Si-Pad

In the past, ionization chambers and proportional counters were used to detect high energy particles like X-rays. As the semiconductor technology advanced, it became possible to measure the movement of electrons in the solid matter, thus helping to the further development of semiconductor detectors. The basic working principle of semiconductor detectors is the same with that of ionization chambers. In semiconductor detectors, first, radiation passes through the depletion layer. There radiation energy changes into electron-hole pairs whose number of pairs is in proportion with the entering radiation. Since the depletion layer area is the result of reverse bias, the created electron-hole pairs are collected in the opposite sides causing them to turn into charges. Collected charges are then sent to the pre-amp which converts them to voltage signals. These signals are also in proportion with the entering radiation. As the final step, these signals are evaluated as a spectrum. This is the simple explanation for the basic working principle of semiconductor detectors.

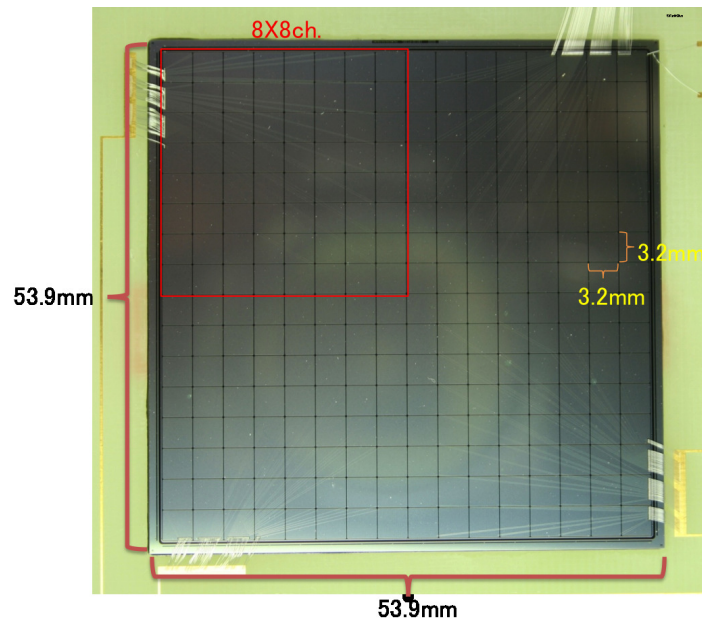


Figure 2.4: Image of Si-Pad

Some examples of the advantages of semiconductor detectors are as follows. In detectors that use gas, like ionization chambers and proportional counters, the energy required for creating an electron-hole pair was more than 100eV, whereas in semiconductor detectors this amount is much lower. For example, in silicon detectors, the energy required for creating an electron-hole pair is 3.64eV. This difference also affects the energy resolution, helping us get more better energy resolution in semiconductor detectors. Another good point of semiconductor detector compared to gas using detectors is its solid state that enables easy handling. As a result, lately, it has become possible to build complex-structured semiconductor detectors.

This development has also led to improved usage of X-ray detectors in various fields. However, due to its low atomic number (14), for Si above 20keV, Compton scattering is more dominant than photon absorption and it makes it hard for silicon to be used in hard X-ray detectors that use photon absorption. On the other hand, in Soft Gamma-ray Detector(SGD), this characteristic becomes valuable, as silicon is used as scatter for Compton camera. Because of the same reason, CdTe, a semiconductor created with two high atomic number elements, is used as absorber in Compton camera in SGD.

The physical characteristics of the Si-Pad in SGD are as follows. One piece of Si-Pad is 5.4x5.4 cm in size with 600um thickness. The main part of the Si-Pad is surrounded by the Guard Ring, an area that helps stabilizing the electric field. In a Si-Pad, there are 256 channels (pads) in total located as 16x16 array. These channels are pad-shaped, where each pad is 3.2x3.2 mm in size. The 256 channels in the Si-Pad are divided into four parts with 8x8 channels in each. The signals from 64 channels (each channel produces a signal) each gathered at the outside corner of their respective parts which are called the Bonding Pads. When gathering at the bonding pads, the signals go through the signal line which is located above the SiO₂, the coating layer of the Si-Pad. The bonding pads are connected to their respective ASICs via aluminium wires. Analog signals from the bonding pads travel to ASIC through these wires and they are changed into digital signals.

Because of the characteristics of the trays used in building the Compton camera, two mirror-symmetrical types of Si-Pad sensors with different signal lines and bonding pads are produced.

One of the electronic characteristics of the Si-Pad sensor is leak current. It is current that flows through the Si-Pad when reverse bias is applied. When the performance of a Si-Pad sensor is being evaluated, leak current is the first thing to be checked. The reasons for the occurrence of leak current are thermal violence and impurities. Leak current causes shot noise signed and it affects the performance of the Si-Pad. As the leak current increases, the noise also gets bigger; and the energy resolution gets worse. Leak current also has temperature dependency. In fully-depletion state Si-Pad sensor (fully-depletion voltage is about 200V), at 20 degrees, leak current is about 100 nA, in -15 degrees, it is about 1 pA. Taking this characteristic into account, the operation temperature of the Si-Pad is determined.

While the bias voltage exceed a critical point, the leak current will become enormous. This situation is called a breakdown. When a breakdown occurs, depletion area will become unable to collect the charges and will stop working as a detector. The creation of an unexpected energy band due to a defected silicon crystal, is one of seasons for breakdown

Another issue affecting the performance of the Si-Pad is capacitance. When the reverse bias is applied to the detector, Si-Pad will become like a charged condenser. In this situation, capacitance si configured upon various factors including the area of the Si-Pad and the size of the depletion area. If the capacitance is large, the energy resolution gets worse.

2.3.2 Status of SGD Si-Pad

The design and the manufacturing process of the SGD Si-Pad is finished. Out of 333 Flight Model Si-Pad sensors manufactured, only 192 will be used in the ASTRO-H satellite. Until the beginning of the manufacture, numerous performance studies were made at different levels, and with the feedback from these studies, the performance was advanced. The Si-Pad at the first stage had 8x16 channels. At this stage, study of the basic characteristics, especially focusing on the performance of a single channel, was done. At the next stage, a Si-Pad called Engineering Model that is the same size as the Flight Model was produced. This stage focused on the evaluation of basic characteristics and multi-channel performance. The study of the Engineering Model showed that the difference of capacitance depending on the signal line of each channel is the reason of unequal performance on energy resolutions. This problem was fixed at the next Pre-Flight Model. In this model, the thickness of the SiO₂ was changed from 1 μ m to 1.5 μ m, and the location of the bonding pads were changed. When the performance evaluation for this model was completed, the manufacturing process for the final Flight Model has started. The Flight Model Si-Pad, combined with four ASICs, will be used in the prototype of the Compton camera. The ground test for the Flight Model Si-Pad will be done via this prototype. Also, to understand the radiation tolerance, tests are being done on Si-Pad sensors selected from each lot.

2.4 Process of multi-channel signal acquisition

To get information from the detected photons, the signals they have been changed into have to be processed with appropriate logic. This signal processing logic must be understood to be able to evaluate the performance of sensors. SGD is using ASICs to process the signals collected from the channels. The simple explanation for the electronic method ASIC uses for signal processing is explained below.

2.4.1 Principal of signal acquisition

When photons reach to the detector, their energies are transformed into charges that convey information. Without appropriate processing, these charges are meaningless by themselves. To acquire information from the charges, steps like signal amplifying and shaping have to be done. At first, charges go to the sensing amp (pre-amp) where they are changed into voltage. With this change, it becomes easier to control and shape the signals. After the pre-amp, signals go to the shaping amp. Here, some corrections regarding their shapes are made. With these corrections, signals become more easily readable by the Analog-Digital Converter (ADC). ADC converts the analog signals to digital ones. These digital signals are actually the energies of the photons detected. The histogram showing the sizes of these energies is called a spectrum. This signal processing logic is the basic for most kinds of signal acquisition methods.

2.4.2 Front end signal process

The ASIC, which is adopted in SGD and HXI, was specially developed for processing signals from semiconductor detectors. It can work with 64 channels at one given moment. Also, like Si-Pad, numerous models have been produced to study its characteristics, and many feedback studies were conducted to come up with the best performance. The flight model ASIC that will be used with Si-Pad sensor is called VA450.3.

The ASIC logic divided for two parts. VA logic is same as that of single signal acquirement, which is consist of pre-amp, shaping amp, ADC. TA logic work as discriminator. When charges come into ASIC, TA logic has judge by its energy, whether it is really photon or not. If the charges enough to trig discriminator, TA logic send acquire signal order to VA logic. By this logic process, SGD can acquire valid photon event and reduce noise data. After the ASIC process, signals pass through FEC, IFC which are provide power to ASIC, and standardization signals to fit DIO board. DIO board is the final step of signal process. In this place signal data compressed and change to suitable for space wire, which is system of communicate with instruments onboard satellite. all after this process, the data saved to coputer, and by analyze them, we can understand about performance of the sensors.

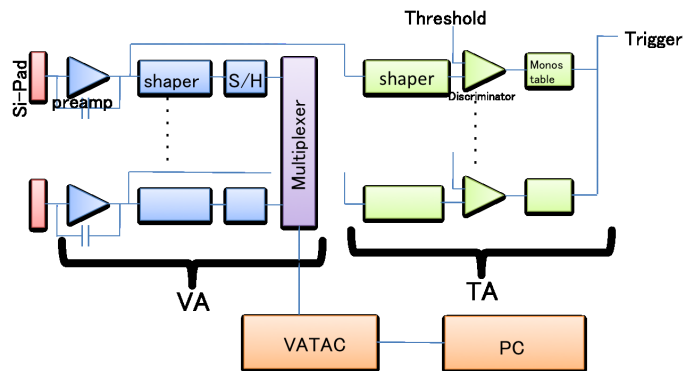


Figure 2.5: Principle of ASIC

Ranking of Flight Model Si-Pad sensors for SGD

Contents

3.1	HPK data	19
3.2	Ranking	20

This chapter will introduce the method of ranking Si-Pad sensors, in order to select ones to be put onboard the actual satellite. After the experiments on the engineer model Si-Pad sensors, 10 pieces of pre-flight model and 333 pieces of flight model Si-Pad sensors were produced. However, SGD uses only 192 pieces of Si-Pad sensors. If produced sensors had perfectly the uniform characteristics and performance, we could just use them randomly. Unfortunately, the Si-Pad sensors have dispersion of performance. Therefore we must sort them according to some properties. After classifying them, we can pick up sensors with the best performance for SGD.

To rank the Si-Pad sensors, we use the leak current data, which was measured by the manufacturer, Hamamatsu Photonics K.K. (HPK). The following sections explain the data and the way we ranked Si-Pad sensors.

3.1 HPK data

Leak current of each sensor was measured after production at HPK. Measured data are divided into two groups. One contains the data of channel leak currents, and the other does the data of guard-ring-leak-currents. In the measurements, one prober is connected to the N⁺ sub pad to provide the reverse bias voltage and the other to each channel of the guardring. The channel-leak current data was measured under 200V of reverse bias, and the guard-ring-leak current data was measured under various bias voltages in the range of 0V to 300V with an interval of 1V. The former can be used to investigate leak current dispersion, and the later can be used to study high-voltage dependency. We must take care of measurement setup. In the orbit, all channels have the same electric field, because they are all connected to ASICs (over vertical ground level). However, in the measurement of the leak current data at HPK, one prober is connected to just one channel. Other channels are isolated from

ground. Therefore, we measured the FM Si-Pad sensor by ourselves to investigate this issue.

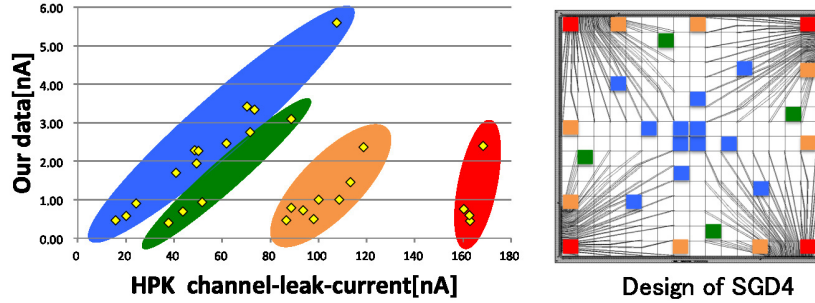


Figure 3.1: Relationship between HPK data and our data

Figure 3.1 compares the HPK data with our measurement data. The data is about SGD4 FM Si-Pad sensor no.39. This sensor was supposed to be used for the experiment about gamma-ray radiation damage. Our measurement was done at 200V and 20 degrees. Unlike the HPK data, all the channels were connected to the ground level. In figure 3.1 left panel, color represents the location of channels as shown in the right panel. The HPK and our data are well correlated. Depending on the position of a channel, the correlations have a different offset. Channels at the center of the Si-Pad (blue ones) have a smaller offset.

3.2 Ranking

By using these channel-leak-current data, this section will introduce how to rank the Si-Pad sensors. First of all, we have to define good sensors. To do that, we look at two characteristics. 1. Less dispersion of leak currents among channels, and 2. Smaller total leak current of all channels. Considering these properties, we analyzed channel-leak-current and ranked the flight model Si-Pad sensors.

First, we derive an average of 256 channel currents on each Si-Pad. In addition, we divide channel current data into 4 parts, like signal readout, and calculate an average on leak current of 64 channels, and a dispersion of four parts. If one part has a significantly different average from other parts, the dispersion is larger. By this method, we pick up bad Si-Pad sensors. After that, we ranked the rest of sensors by the total channel-leak-current. However this method have failed. Since the intrinsic current-leak-current dispersion on each sensor is not small, even for the normal Si-Pad, the average and dispersion are not largely affected by channel.

To avoid the above case, we normalize each of channel current by the average current of the same channel over all sensors. We define this as a formula 3.1

$$\bar{I}(ch) = \frac{\sum_{sensor=1}^n I(sensor, ch)}{n} \quad (3.1)$$

In the formula, $I(sensor, ch)$ represents channel-leak-current, where the "sensor" represents the Si-Pad number, and the "ch" represents the channel number.

Then we normalized the current of each channel as,

$$I_{stand}(sensor, ch) = \frac{I(sensor, ch)}{\bar{I}(ch)} \quad (3.2)$$

and calculate the dispersion of the normalized current among channels in one Si-Pad as,

$$I_{dis}(sensor) = \frac{\sum_{ch=1}^{256} (I_{stand}(sensor, ch) - \frac{\sum_{ch=1}^{256} I_{stand}(sensor, ch)}{256})^2}{256} \quad (3.3)$$

This evaluation considers the intrinsic current dispersion, caused by the position-dependent current value, the near-GR channels has a large current. This method provides more accurate data compared to the former method. Figure 3.2 shows the result of this calculation.

The red data represents the first lot of FM Si-Pad, and the blue represent the second lot. Figure 3.3 shows channel-leak-current map. When the dispersion is large, the leak current map shows an abnormal pattern. On the other hand, when dispersion is small, map shows a uniform pattern.

Apart from the above normalized dispersion of channel current, we additionally consider the total current between the n- sub and GR, for ranking.

Figure 3.4 shows the correlation between the normalized and the total current. The total leak current is the value of guard-ring-leak-current at 200V. These two currents have a correlation. This relation helps to select good sensors.

The primary-ranked sensors are surrounded by the green blacks. These 128 pieces of each type of Si-Pad sensors are used for the 8 flight model Compton cameras, including 2 spare cameras. The secondary-ranked sensors are surrounded by the blue blocks, and they are used for the engineer model of one Compton camera. Other sensors are defined as bad sensors and they are used to study the radiation damages and else.

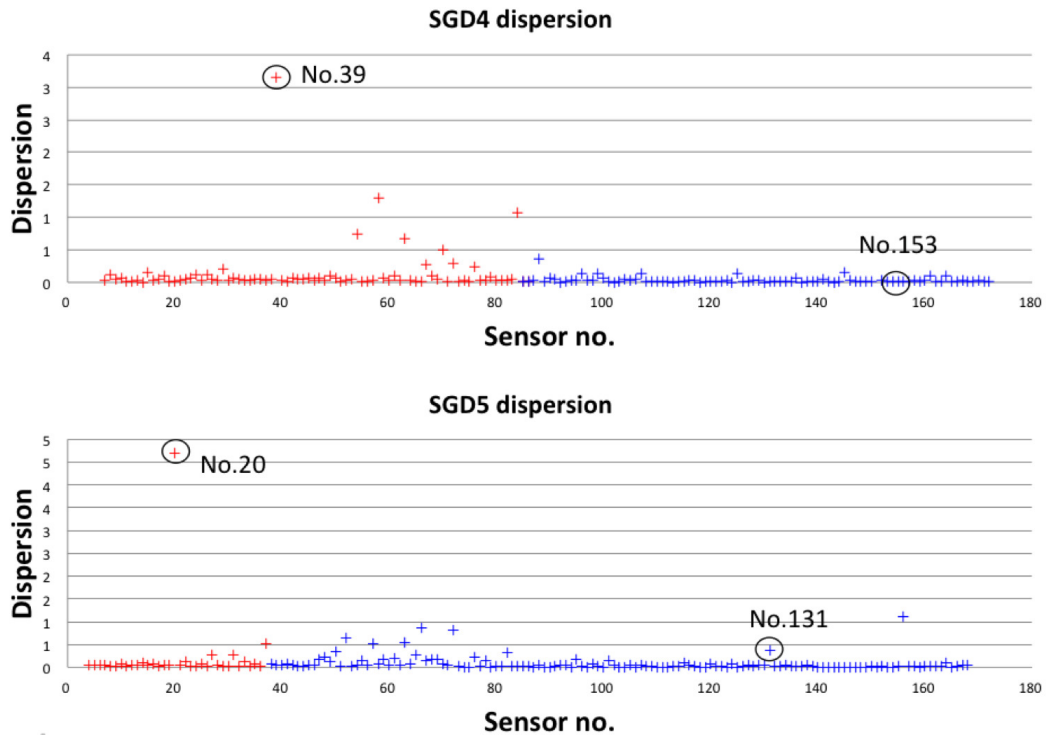


Figure 3.2: Dispersion of normalized channel current of FM Si-Pad

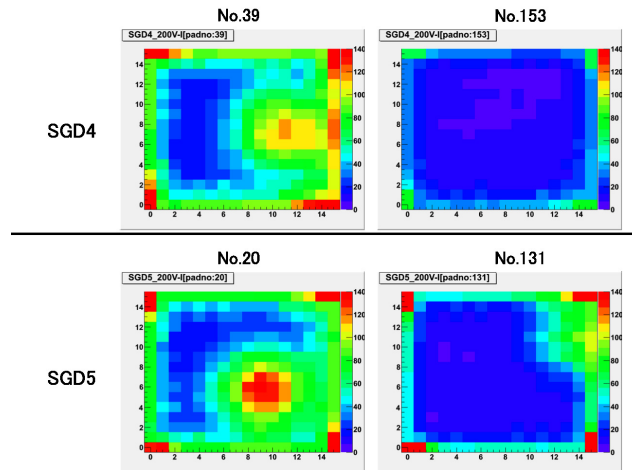


Figure 3.3: Example of leak current maps

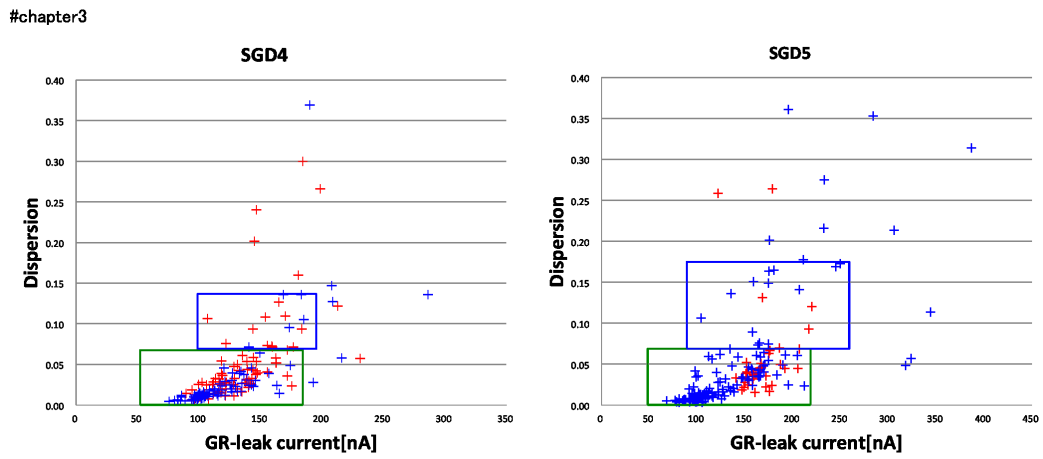


Figure 3.4: Correlation between the normalized and the total current of the type SGD4(left) and SGD5(right)

Performance Evaluation of Si-Pad sensors with ASIC

Contents

4.1	Items of Performance Evaluation	25
4.1.1	Dependence on Bias High Voltage	25
4.1.2	Temperature Dependence	25
4.2	Expected Result of the PFM Si-Pad sensors	26
4.2.1	Multi-channel readout of PFM Si-Pad with VA450.3	26
4.2.2	Single-channel readout with FM Si-Pad sensor	30
4.3	Results on the FM Si-Pad sensor	32
4.3.1	Experiment Setup	32
4.3.2	High voltage dependency	32
4.3.3	Temperature Dependency	35

In this chapter, we evaluate the Si-Pad sensor performance by multi-channel signal readout, especially, on the high-voltage and temperature dependences. For this evaluation, we use the final versions of Si-Pad sensor and ASIC.

4.1 Items of Performance Evaluation

4.1.1 Dependence on Bias High Voltage

Semiconductor sensors are known to show a bias voltage dependence of properties, such as a depth and structure of depletion layer, leakage current. These properties are ideally stable from the full depletion voltage to the breakdown voltage, but they are not exactly stable. For example, the edge of the depletion layer still evolves in this voltage range, and thus the sensor properties at the sensor edge could be affected. Therefore, we investigate the high voltage dependence of Si-pad sensors.

4.1.2 Temperature Dependence

Noise characteristics of Si-Pad sensors get smaller when the temperature is lower. This characteristic means that the spectrum performance gets better at lower temperature. The operation temperature of Si-Pad in the orbit depends on the thermal

design of SGD, and therefore, it is important to study the temperature dependence of Si-Pad to finalize the SGD design. For these reasons, we investigate the temperature dependency of Si-Pad sensors.

4.2 Expected Result of the PFM Si-Pad sensors

4.2.1 Multi-channel readout of PFM Si-Pad with VA450.3

First, we used the SGD4 no.3 Si-Pad and the ASIC VA450.3. The ASIC was connected to the 8x8 pads, which stands for 1/4 of the Si-Pad sensor. The ASIC VA450, the old version of ASIC, was also connected to another 8x8 pads, but VA450 had some bug, which made an unstable pulse peak shaped branch. Therefore, we could not evaluate sensor with this ASIC. At the final step, this setup consists of one PFM Si-Pad and two ASICs. Half of channels that are connected to ASICs are on the same electric voltage as ground. The other half of the channels are not connected to anywhere, they are electrically floated. So, it is not perfectly the same condition as the orbit. We did not analyze channels which are close to floated channels to avoid the effect of unstable electric field. This setup was constructed by Watanabe in ISAS, and Tanaka in SLAC, and the experiment was performed at Nagoya University.

The setup was located in an aluminum box. The box was set in the thermal chamber to keep the temperature stably low at -10 degrees. Outside of the thermal chamber, two regulated power supplies, a high voltage supply and a DIO board, are equipped to operate the detector. Data were from DIO board to computer via the space-wire. Input parameters of ASIC in this experiment are summarized in the appendix.

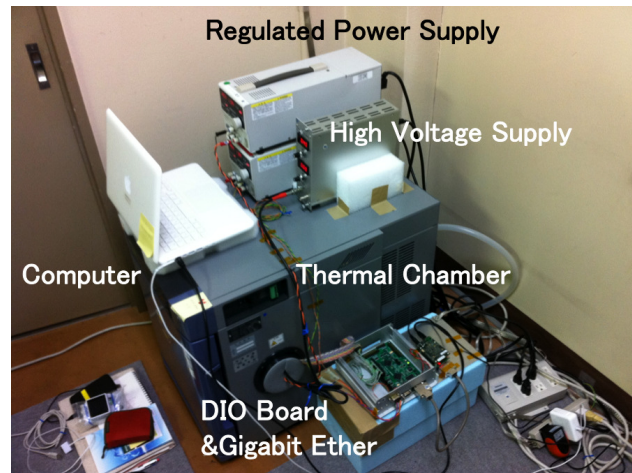


Figure 4.1: Setup of PFM SiPad measurement(1)

With this setup, the high voltage was scaled from 100V to 400V at -10 degrees.

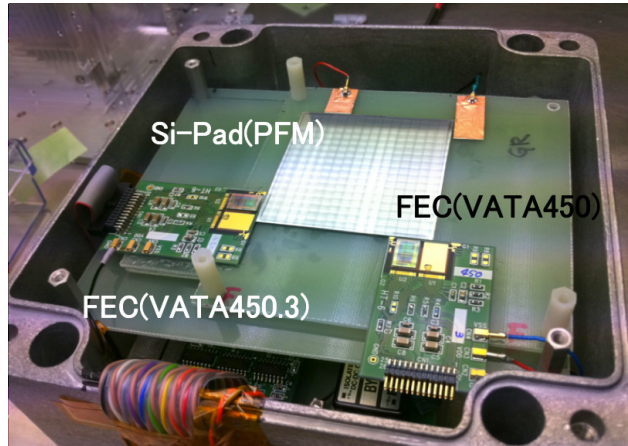
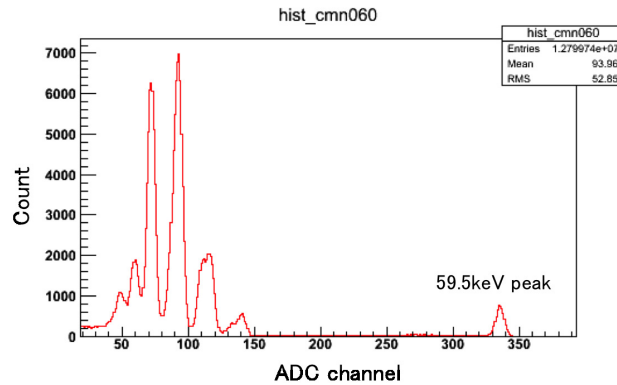


Figure 4.2: Setup of PFM SiPad measurement(2)

Also the temperature dependency was measured from -25 degrees to -10 degrees at 200V. For evaluation, ^{241}Am was used as a gamma-ray source, from which the 59.5keV gamma-ray is useful to evaluate the Si-Pad sensor. Figure 4.3 is an example of spectra that was taken. The peak was fit by a Gaussian, and we used a Full Width Half Mean (FWHM) as an indicator of the spectrum performance.

Figure 4.3: Spectrum of ^{241}Am of one channel

At first, for high voltage dependency, we evaluated the dispersion, map and histogram of spectral energy resolution. Figure 4.4 is a resolution map of each high voltage. In the map, one pixel corresponds to each channel pad of the Si-Pad sensor. The color presents the energy resolution. Red-colored area have about 2.5keV energy resolution, and the spectral performance in this area is worse than other green or blue area. In the figure 4.4, four maps have commonly worse area(right lower part). Signal lines from other channels run on this area and thus affect the performance. On the right and bottom side, the guarding surrounds the sensor. This structure

affects something worse to the neighboring channels. Also when high voltage was up to 400V, the left side of channels got worse. Region at the left of area is flouted. This could affect the performance.

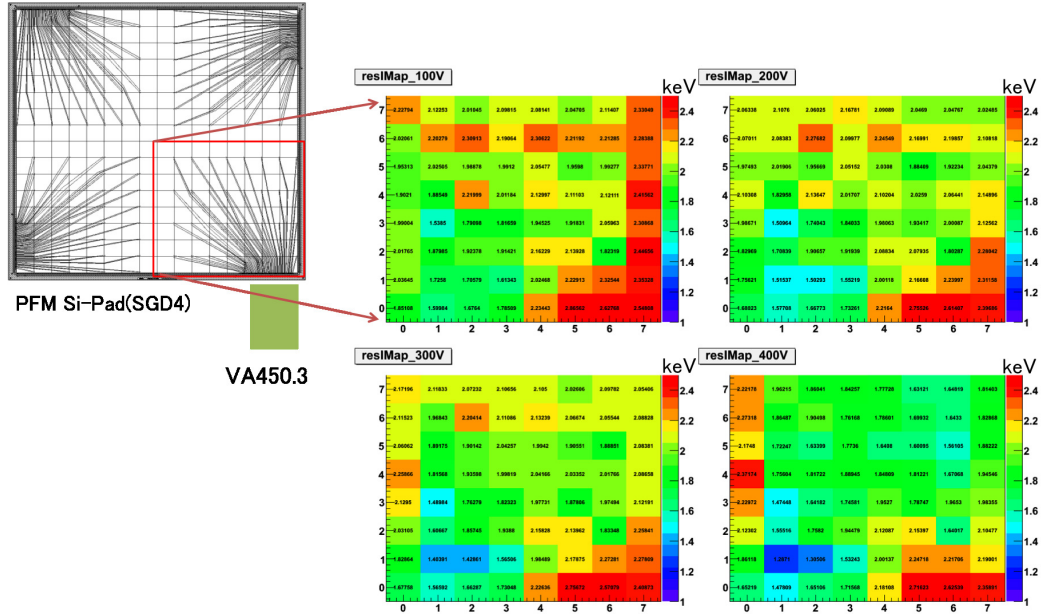


Figure 4.4: Resolution map from 100V to 400V

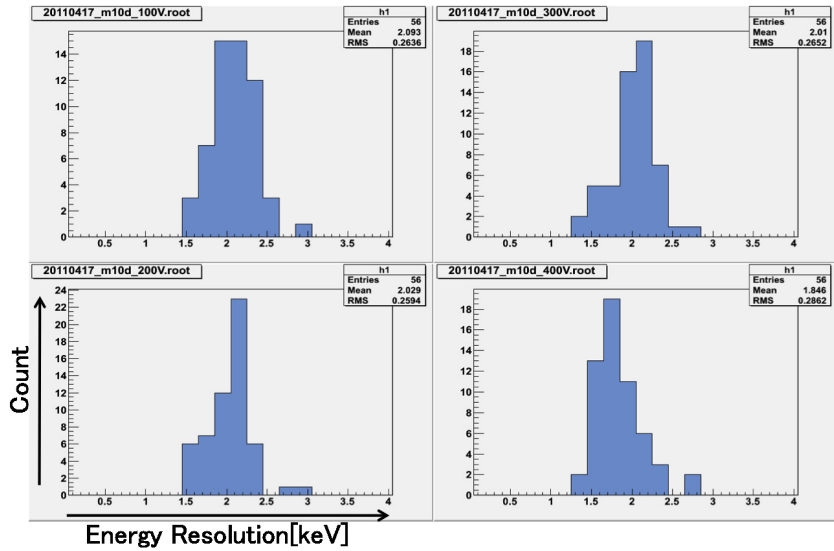


Figure 4.5: Histogram of energy resolution at each bias voltage

Figure 4.5 is a histogram of energy resolution. In this histogram, due to the

affection of flouted area, the left side channels are excluded. The average of energy resolution at each voltage is plotted in figure 4.6. This graph means that higher high voltage bring better performance. Especially, around 300V, the resolution dramatically goes better. However, looking at individual energy resolution (figure 4.7), we cannot find common characteristics of high voltage dependency. Some channels showed getting better performance, some channels did not.

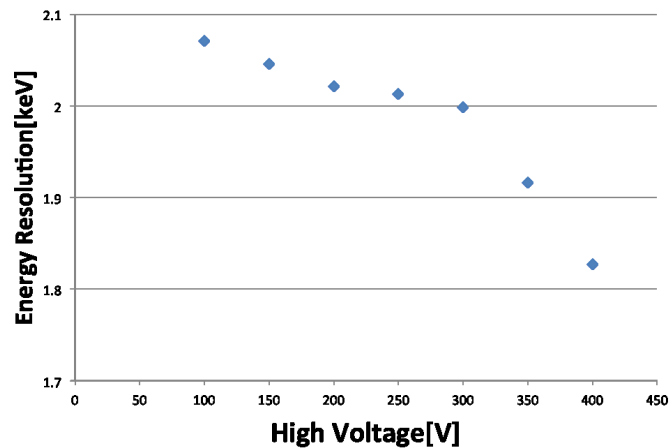


Figure 4.6: Energy resolution averaged over channels against the bias voltage

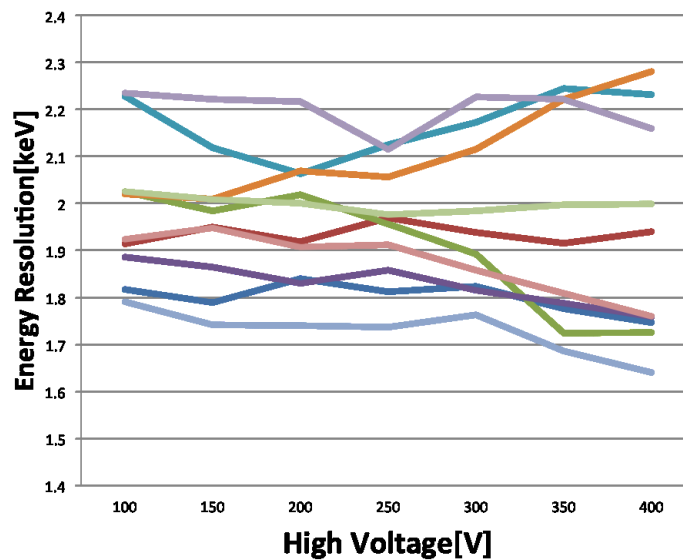


Figure 4.7: Energy resolution of individual channels against bias voltage

Figure 4.8 is a histogram of energy resolution at various temperatures. This

histogram have little tendency that the energy resolution becomes better at lower temperature.

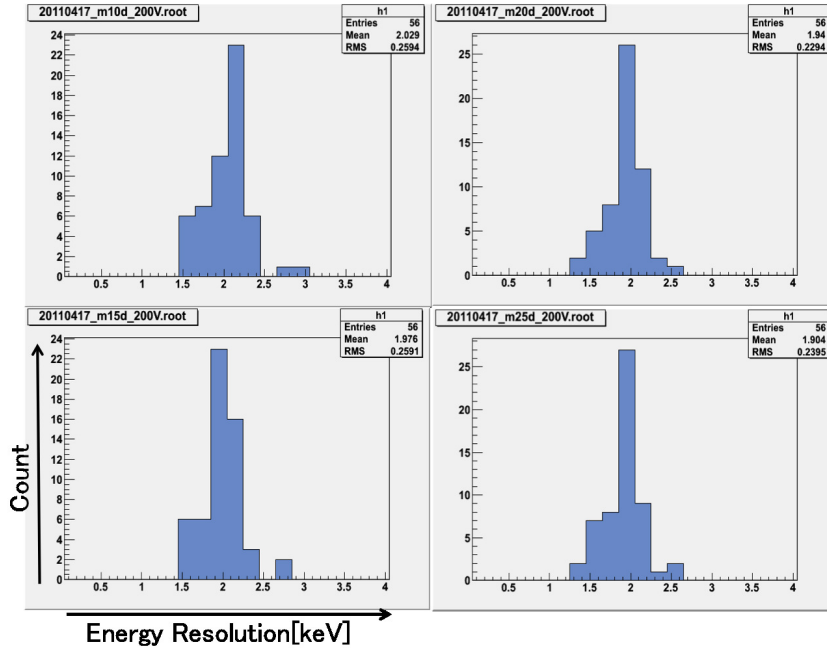


Figure 4.8: Histogram of energy resolution at each temperature, -10degree, -15degree, -20degree, -25degree

In this experiment, we can get the macroscopic characteristics of high voltage and temperature dependency. However, we cannot be confident about these results, because of the effect of the floated area.

4.2.2 Single-channel readout with FM Si-Pad sensor

The conclusion of the former subsection is that more precise setup is needed to evaluate the performance of Si-Pad. In this subsection, we fix the former setup problem. This FM Si-Pad(SGD4 no.39) is used to study the gamma-ray radiation damage. Instead of ASIC, we use conventional preamp CP580K and a shaping amp ortec572, to readout one channel. All channels other than one readout channel are connected to the ground. Therefore, we can measure the spectrum under almost the same electrical stable condition. Before the sensor irradiated, we measure the high voltage and temperature dependency of one channel pad.

Figure 4.9 and figure 4.10 show the high voltage and temperature dependency. Results of this single-channel performance evaluation are almost consistent with the expected one.

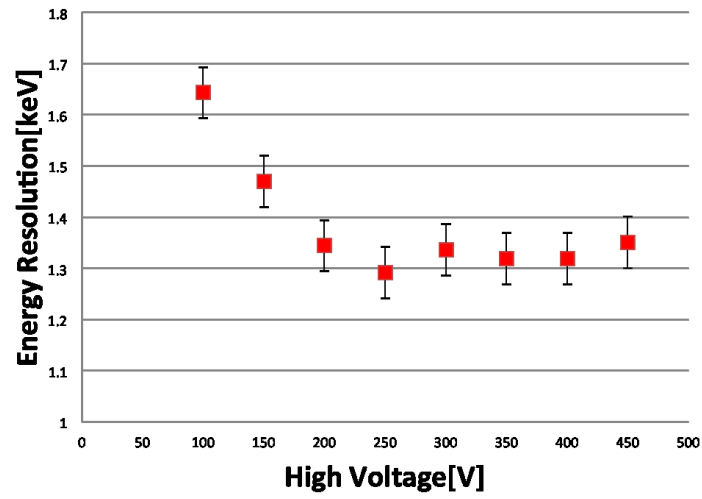


Figure 4.9: Energy resolution of one channel against high voltage dependency

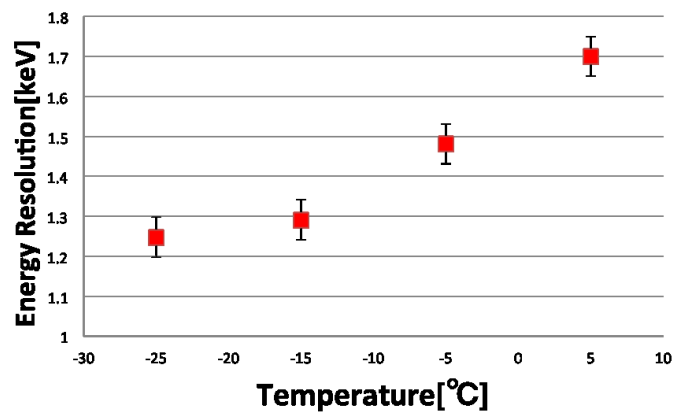


Figure 4.10: Energy resolution of one channel against temperature dependency

4.3 Results on the FM Si-Pad sensor

In this section, using a FM Si-Pad, we evaluate the high voltage dependency

4.3.1 Experiment Setup

Setup for this experiment is different from that of the previous experiments. Instead of the hand-made acrylic plate, we use FM-type tray for the Si-Pad. The tray is designed to assembly a Compton camera. Two Si-Pad sensors(SGD4:No.68, SGD5:No.33) and 8 ASICs are attached on both sides of tray. This tray unit will be used for the engineering model of Compton camera. The setup was constructed in Mitsubishi Heavy Industries, Ltd(MHI). Therefore, handling of this setup, such as operation time or bias high voltage, is very strict.

4.3.2 High voltage dependency

4.3.2.1 Analysis of Pedestal Data

Because the setup has 512 channels, speed of signal readout is very slow, compared with the former experiment, which has 64 channels. For this reason, it takes long time to obtain enough events for analysis. First, we evaluated the pedestal data. This data is used to evaluate the noise property. By comparing pedestal data among different high voltage, we could know the high voltage dependency of noise. We took the data from 200V to 320V at -15degree. When the pedestal is fitted with gaussian, the gaussian sigma represents the nose. We divided the sigma at 290V by that of 200V, and plotted them in Figure 4.11. In the figure 4.11, we can see two peaks.

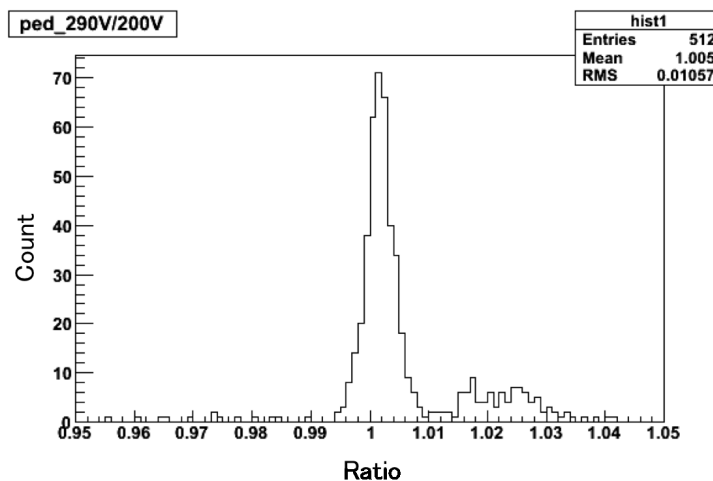


Figure 4.11: Histogram of Pedestal sigma ratio

To find the reason of two peaks, we draw a map of the ratio of sigma(Figure 4.12). Considering the result of the PFM Si-Pad evaluation, we can guess that the

left peak is due to the channels close to the guardring. Figure 4.13 is the same histogram, but the channel data near the guardring are removed. We can confirm that the left peak is also removed. From this result, the channels close to the GR are found to be sensitive to the high voltage.

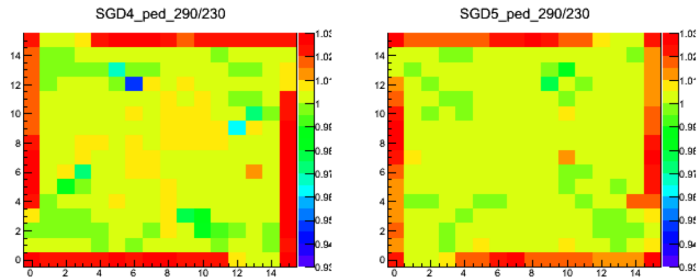


Figure 4.12: Map of Sigma ratio of the type SGD4(left) and SGD5(right)

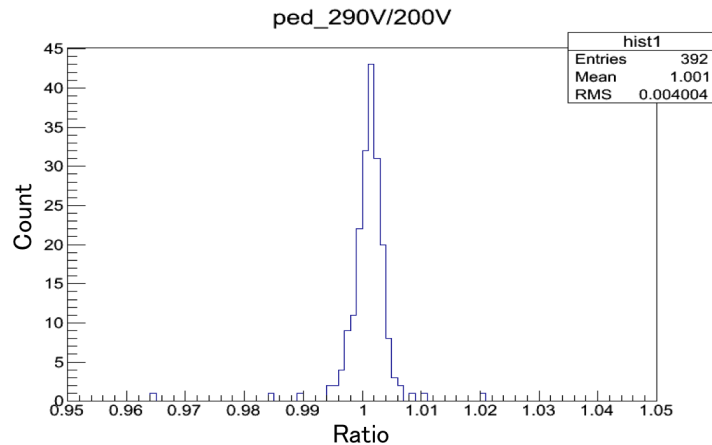


Figure 4.13: Histogram of Pedestal sigma without near GR channels

We analyze the pedestal data of other high voltage without near-GR channels data. Figure 4.14 shows the result. From 200V to 320V, the sigma is almost stable within 1 percent. This is consistent with the single-channel performance evaluation.

4.3.2.2 Analysis of ^{241}Am data

Although the pedestal data contain noise property, the best way to evaluate spectral performance is to analyze the gamma-ray source data. The low event rate, due to lots of channels, is the most problem of measurements. However, by changing the ASIC mode to eliminate pedestal data, it can be possible to fasten the speed of signal acquisition. Figure 4.15 is a histogram of energy resolution of 59.5keV at

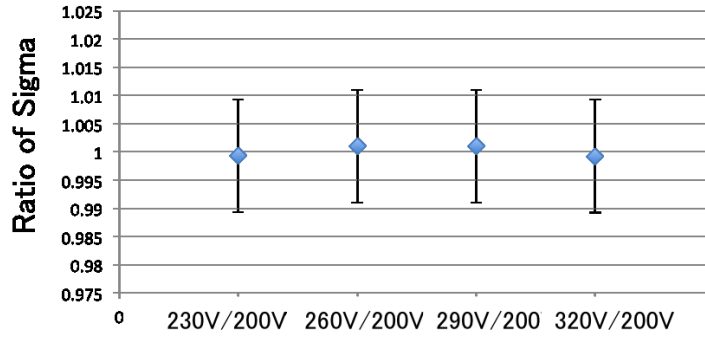


Figure 4.14: Pedestal sigma ratio at various high voltage

230V, 280V, 330V. Figure 4.16 is the average energy resolution over channels in figure 4.15. We can say that the high voltage dependency is small.

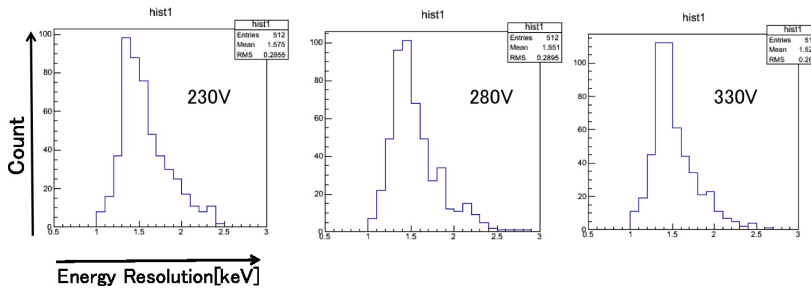


Figure 4.15: Histogram of energy resolution

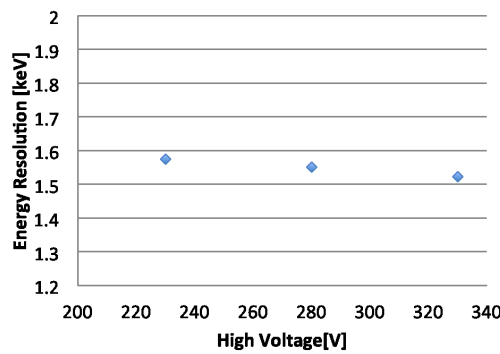


Figure 4.16: Relation between HV and energy resolution

When analyzing pedestal data, we expect that the channels are affected by the guardring. Also in this section, we investigate the affect of the guardring. At first, we divide 2 pieces of Si-Pad into 8 sections(chip0-chip7) corresponding to their

ASICs. In addition, we analyze by separating and take apart the inner channels(not affected by the GR) and the outer channels(affected by the GR)(4.17). Their spectrums are merged for statistically more accurate analysis. Figure 4.18 shows the result of this analysis. The graph is divided by sections, and the plots represent energy resolution depending on bias(230V, 280V, 330V). This graph shows that the channels affected by the guardring have high-voltage dependency. When bias-high-voltage goes up, the energy resolution gets better.

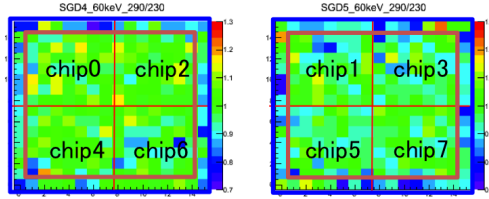


Figure 4.17: 59.5keV peak nergy resolution map and partition of Si-Pad

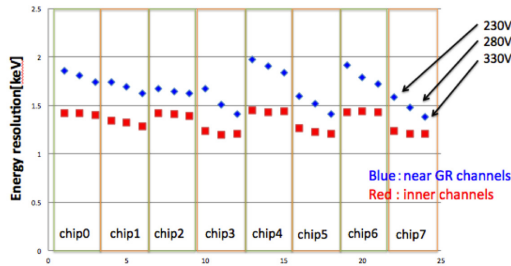


Figure 4.18: Affect of GR on HV dependency

4.3.3 Temperature Dependency

Next, we investigate the temperature dependency of Si-Pad. Figure 4.19, and figure 4.20 show the results of analysis. The experiment temperature is 5 and -10degree at 250V, and -15degree at 230V.

The performance changes seen due to the temperature are clear. When the temperature goes up, the spectrum performance gets worse. The same result was found in calculations done with the noise model. The noise model is used for calculating the effect of spectrum performance by leak current and capacitance. The formula for the noise model is as follows.

$$\Delta E_{noise} = \sqrt{(2 \times e \times I[A] \times \alpha \times \tau[\mu s] \times (2.355 \times 3.64 \times 10^{-3}/e)^2) + (0.55 + 0.16 \times C[pF])^2} \tag{4.1}$$

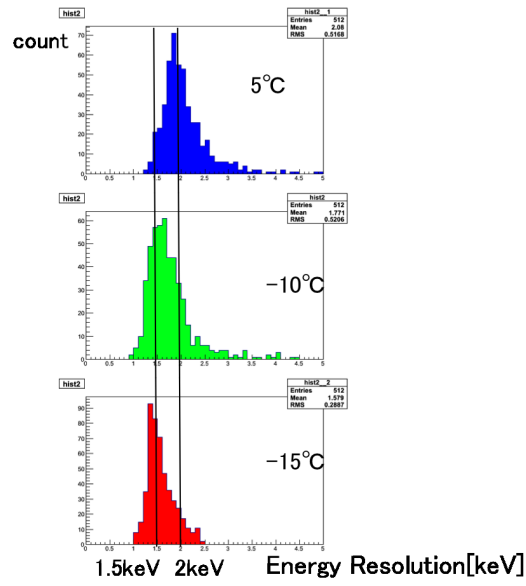


Figure 4.19: Histogram of energy resolution of each channel at various temperature

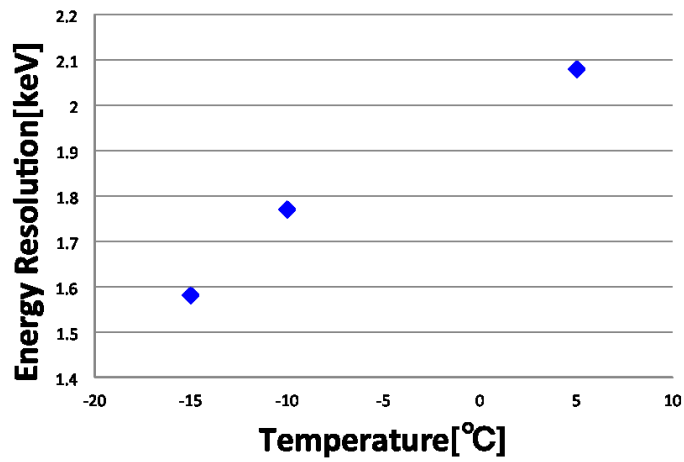


Figure 4.20: Relation between temperature and energy resolution average over all channels

Figure 4.21 shows the temperature dependencies of single-channel-readout, multi-channel-readout and noise model. The graph shows that the three of them have the same tendency. Therefore, the energy resolution behaves as we expected. With these results, we can confirm that the Si-Pad sensors satisfy the energy resolution requirement of $\Delta E < 2\text{keV}@-10\text{degree}$.

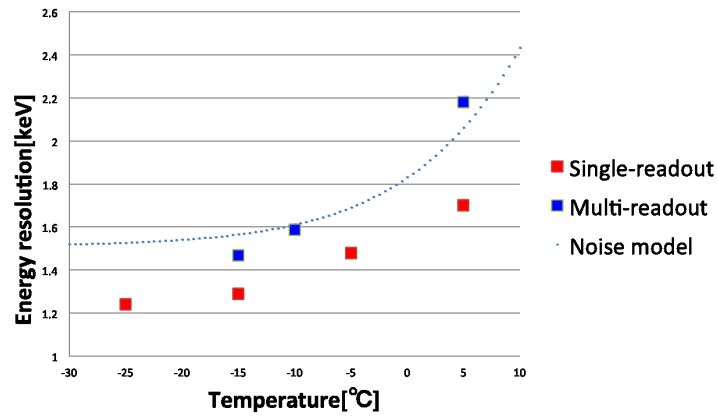


Figure 4.21: Temperature dependency of energy resolution for the data and model

Consideration

In this thesis report, we studied Si-Pad sensors for soft gamma-ray detector (SGD) which will be mounted on the the next generation astronomy observation satellite ASTRO-H. The design and production of the Si-Pad which is used as Compton scatter for the Soft Gamma-ray Photon was over.

In this study, we came up with the criteria to classify Si-Pads according to the quality of their leak current, and we selected the sensors that can actually be used in the SGD. We also studied the HV and temperature dependency of the final model Si-Pad with multi-channel readout.

Regarding HV dependency, we saw that most channels show a stable spectral performance above the fully depletion voltage regardless of the HV dependency. However, we found the existence of HV dependency on the outer channels resulting from the effect of the Guradring. This result has become a guideline for determining the HV dependency of the Si-Pad that will be mounted on the satellite. Also examining the temperature dependency, we found similar results with the theoretical model results, which confirmed that the Si-Pad meets the required performance.

Our results are the first performance evaluation data of Flight Model Si-Pads, giving us the starting guidelines for further development of future detectors.

As the next step, radiation damage and detection efficiency of the Si-Pad will be studied to evaluate the response as a detector.

Bibliography

- [1] <http://www.nasa.gov/vision/universe/starsgalaxies/chandra7years.html>
 - [2] sci.esa.int/xmm
 - [3] <http://www.astro.isas.ac.jp/suzaku/index.html.ja>
 - [4] <http://astro-h.isas.jaxa.jp/gallery/satelite/05e.html>
 - [5] <http://astro-h.isas.jaxa.jp/researchers/GakkaiAki2011/W55a-yoshitaka-ishisaki.pdf>
 - [6] <http://www.mext.go.jp/component/b-menu/shingi/toushin/-icsFiles/afieldfile/2010/05/28/1291500-4.pdf>
 - [7] <http://www.mext.go.jp/component/b-menu/shingi/toushin/-icsFiles/afieldfile/2010/05/28/1291500-4.pdf>
 - [8] <http://astro-h.isas.jaxa.jp/researchers/SPIE2010/SPIE2010-7732-40.pdf>
 - [9] <http://astro-h.isas.jaxa.jp/researchers/GakkaiAki2011/W60a-Hiroyoshi-Kato.pdf>
 - [10] 2011year Noda Master thesis
 - [11] <http://www.nustar.caltech.edu/news/33/71/final-deployment/d,gallery-detail-template>
 - [12] <http://gems.gsfc.nasa.gov/gallery-spacecraft.html>
 - [13] <http://www.brera.inaf.it/NHXM/index.php5/About-NHXM>
 - [14] <http://www.cospa.ntu.edu.tw/aappsbulletin/data/19-2/36HXMT.pdf>
 - [15] <http://gri.cesr.fr/documents/eslab.pdf>
 - [16] <http://www.gamma.mpe-garching.mpg.de/MEGA/documents/papers/Portland-ImagingProperties.pdf> (Cited on page 1.)
(Cited on page 1.)
- (Cited on page 1.)

(Cited on page 2.)

(Cited on pages 3 and 4.)

(Not cited.)

(Cited on page 5.)